THE JOURNAL OF PHYSICAL CHEMISTRY A
A JOURNAL OF THE AMERICAN CHEMICAL SOCIETY

pubs.acs.org/JPCA

Article

Mode-Specific Quantum and Quasi-Classical Trajectory Dynamics of the $F^- + CH_3I \rightarrow I^- + CH_3F$ S_N2 Reaction

Yan Wang,* Zhao Tu, Gábor Czakó,* Hongwei Song, and Minghui Yang

Cite This: *J. Phys. Chem. A* 2025, 129, 6344−6349

Read Online

ACCESS | Metrics & More | Article Recommendations

ABSTRACT: Bimolecular nucleophilic substitution (S_N2) reactions in the gas phase are of great importance in chemistry, whose microscopic mechanisms are, however, not comprehensively understood. In this work, the mode-specific quantum dynamics of the prototypical S_N2 reaction $F^- + CH_3I \rightarrow I^- + CH_3F$ are investigated using reduced six-dimensional quantum wave packet and full-dimensional quasi-classical trajectory methods. The reaction probabilities are calculated for both the ground and excited vibrational states of the reactant CH_3I at collision energies up to 2.3 eV. The results show that the CH stretching vibration slightly suppresses the reaction with collision energies below 0.4 eV, becomes a spectator mode in the collision energy range of 0.4−1.5 eV, and then enhances the reaction at higher collision energies.

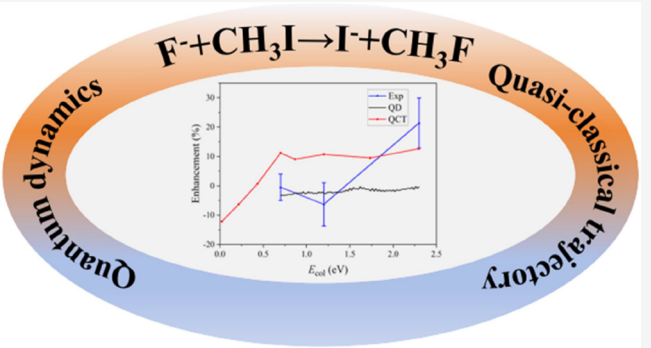

1. INTRODUCTION

Selectively cleaving chemical bonds and steering reaction outcomes represent enduring pursuits in chemistry.[1,2] Mode specificity, characterized by the dependence of reactivity on excitation of distinct ro-vibrational modes, provides a powerful approach for harnessing and controlling reactions.[3−11] Polanyi established empirical rules for triatomic reactions decades ago, correlating the relative efficiency of vibrational and translational energy with the location of the transition state on the reaction path.[12] Vibrational mode selectivity in polyatomic reactions, however, becomes much more complicated owing to the presence of multiple vibrational modes involving collective atomic motions. A given vibrational mode may act as a spectator, exerting negligible influence, or modulate reactivity by either enhancing or suppressing the reaction. In this regard, significant efforts have been devoted to elucidate mode-specific dynamics in polyatomic systems, exemplified by X + H_2O/HDO, CH_4/CHD_3, and C_2H_6, with X = H, F, Cl, O, and Br, given their pivotal roles in combustion, atmospheric, and astrophysical chemistry.[3,13−18]

For ion−molecule reactions, understanding mode specificity is comparatively difficult, primarily due to the presence of submerged barriers and long-lived entrance-channel complexes.[19] Tasi and Czakó carried out a detailed investigation on the vibrational mode-specific dynamics in the $OH^- + CH_3I$ reaction, revealing the impact of different normal-mode excitations in the reactants on reactivity, mechanism, and energy distribution.[20] Furthermore, ion−molecule reactions of the type $X^- + CH_3Y \rightarrow XCH_3 + Y^-$ [X, Y = F, Cl, Br, I] have been studied extensively as they represent model systems for bimolecular nucleophilic substitution (S_N2) reactions.[10,21−28] The potential energy surfaces (PESs) for these reactions are usually complicated, which have many stationary points such as pre- and postreactive ion−dipole complexes and saddle points between them.[22,29−33] Early pioneering work based on quasi-classical trajectory (QCT) simulations demonstrated that some mode-specific vibrational excitations can enhance S_N2 reactivity.[34,35] Previous experimental and theoretical investigations of the $Cl^- + CH_3Cl$ and $Cl^- + CH_3Br$ S_N2 reactions provided evidence for nonstatistical behavior and the vibrational mode-specific reactivity enhancement effect.[34,36−38] For the $Cl^- + CH_3I$ S_N2 reaction, recent quantum wave packet dynamics calculations predicted a change from rate enhancement to rate reduction with increasing collision energy upon excitation of the C−I bond.[39] For the $F^- + CH_3Cl$ S_N2 reaction, QCT results indicated a modest rate enhancement by exciting the CH stretching vibration, whereas quantum dynamics (QD) calculations suggested inhibition upon CH stretching excitation. Both QD and QCT results exhibited a strong collision energy dependence.[21] For the $F^- + CH_3I$ S_N2

Received: May 8, 2025
Revised: June 25, 2025
Accepted: June 26, 2025
Published: July 7, 2025

Downloaded via UNIV OF SZEGED on September 10, 2025 at 14:15:48 (UTC).
See https://pubs.acs.org/sharingguidelines for options on how to legitimately share published articles.

© 2025 American Chemical Society

https://doi.org/10.1021/acs.jpca.5c03163
J. Phys. Chem. A 2025, 129, 6344−6349

reaction, crossed-beam experiments and/or QCT theory revealed that vibrational excitation of the symmetric CH stretching mode significantly promotes proton transfer and double-inversion processes at low collision energies while having the modest enhancement effects on the S_N2 reaction at higher collision energies.[23,28] Recently, in collaboration with the research groups of Wester and Czakó, we investigated the dynamic isotope effects in the $F^- + CH_3I/CD_3I$ S_N2 reaction. The observed significantly enhanced forward scattering for hydrogenated reactants compared to their deuterated counterparts was attributed to quantum tunneling effects.[40]

In this work, we present a combined QD and QCT investigation of the dynamics of the $F^- + CH_3I \rightarrow CH_3F + I^-$ reaction. The quantum dynamics employs a six-dimensional (6D) Hamiltonian reduced from the Palma−Clary model, which keeps the CH_3 group maintaining its C_{3v} symmetry in the reaction. The accurate global potential energy surface developed by Czakó and co-workers was utilized in the calcualtions.[22] The paper is structured as follows: Section 2 and 3 outline the theoretical methodologies. Results and discussion are presented in Section 4, followed by a brief conclusion in Section 5.

2. QUANTUM DYNAMICS

The 6D model for the $X^- + CH_3Y$ system has been employed in the study of the $F^- + CH_3I$ S_N2 reaction dynamics. The Jacobi coordinates employed in this work are shown in Figure 1. Here, **R** denotes the vector connecting the center of mass of

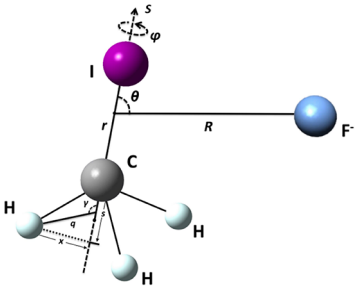

Figure 1. Jacobi coordinates for the six-dimensional model for the F^- + CH_3I reaction.

CH_3I and F^-, which also serves as the z-axis of the body-fixed (BF) frame, and r signifies the vector joining the center of mass of CH_3 and I, which coincides with the C_{3v} symmetric axis S. The symmetric CH stretching mode and the umbrella mode of the CH_3 group are characterized by the scaled-polar coordinates (ρ, γ), used to describe the rotation of CH_3I. The scaled-polar coordinates for the CH_3 group are defined as $\rho = \sqrt{x^2 + y^2}$ and $\gamma = \pi - \arctan\frac{x}{y}$, with $y = \sqrt{m_C/(m_C + 3m_H)}s$, where x represents the distance from one of the H atoms to the C_{3v} symmetry axis S and s is the distance from the C atom to the centroid of the three H atoms.

The 6D model Hamiltonian for the $F^- + CH_3I$ reaction is expressed as ($\hbar = 1$):

$$\hat{H} = -\frac{1}{2\mu_R}\frac{\partial^2}{\partial R^2} + \frac{(\hat{J}_{tot} - \hat{J})^2}{2\mu_R R^2} + \hat{K}^{vib}_{CH_3I} + \hat{K}^{rot}_{CH_3I} + V(R, r, \rho, \gamma, \theta, \varphi) \quad (1)$$

where μ_R is the reduced mass of the system, $\hat{J}_{tot}$ is the system's total angular momentum operator, and $\hat{J}$ represents the rotational angular momentum operator of CH_3I. $\hat{K}^{vib}_{CH_3I}$ and $\hat{K}^{rot}_{CH_3I}$ correspond to the vibrational and rotational kinetic energy operators of CH_3I, respectively. The last term $V(R, r, \rho, \gamma, \theta, \varphi)$ in the Hamiltonian is the potential energy operator.[22]

The vibrational and rotational kinetic operators for the CH_3I monomer defined in the (ρ,γ) coordinate system are written as

$$\hat{K}^{vib}_{CH_3I} = -\frac{1}{2\mu_r}\frac{\partial^2}{\partial r^2} - \frac{1}{2\mu_x}\left(\frac{\partial^2}{\partial \rho^2} + \frac{1}{\rho^2}\frac{\partial^2}{\partial \gamma^2} + \frac{1}{4\rho^2}\right) \quad (2)$$

where μ_r is the CH_3−I reduced mass and $\mu_x = 3m_H$. The rotation of CH_3I is described by a symmetric-rotor Hamiltonian with C_{3v} symmetric axis S as the z-axis

$$\hat{K}^{rot}_{CH_3I} = \frac{1}{2I_A}\hat{J}^2 + \left(\frac{1}{2I_C} - \frac{1}{2I_A}\right)\hat{J}_z^2 \quad (3)$$

where $\hat{J}$ denotes the rotational angular momentum operator of CH_3I and $\hat{J}_z$ is its z-component. The principal moments of inertia I_A and I_C are defined as

$$I_A = \frac{m_I(m_C + 3m_H)}{m_I + m_C + 3m_H}r^2 + \frac{3m_C m_H}{m_C + 3m^H}s^2 + \frac{3}{2}m_H x^2 \quad (4)$$

$$I_C = 3m_H x^2 \quad (5)$$

The time-dependent wave function is expanded using the parity-adapted BF rotational basis functions $\Phi^{J_{tot}MK\varepsilon}_{JK}$ as

$$\Psi^{J_{tot}M\varepsilon} = \sum_{n_R,n_r,n_\rho,n_\gamma}\sum_{KJk} c^{J_{tot}MK\varepsilon}_{n_R n_r n_\rho n_\gamma Jk}(t)G_{n_R}(R)F_{n_r}(r)Q_{n_\rho}(\rho) H_{n_\gamma}(\gamma)\Phi^{J_{tot}MK\varepsilon}_{Jk}(\hat{R}, \hat{r}) \quad (6)$$

and

$$\Phi^{J_{tot}MK\varepsilon}_{Jk} = \sqrt{\frac{1}{2(1 + \delta_{\bar{K}0}\delta_{k0})}}\left[\overline{D}^{J_{tot}}_{M\bar{K}}(\hat{R})\overline{D}^{J}_{\bar{K}k}(\hat{r}) + \varepsilon(-1)^{J_{tot}+k}\overline{D}^{J_{tot}}_{M-\bar{K}}(\hat{R})\overline{D}^{J}_{-\bar{K}-k}(\hat{r})\right] \quad (7)$$

where $\bar{K} = |K|$ and ε specifies the wave function's parity under space inversion. $\overline{D}^{J_{tot}}_{M\bar{K}} = \sqrt{\frac{2J_{tot}+1}{8\pi^2}}D^{J_{tot}*}_{MK}$ and $\overline{D}^{J}_{\bar{K}k} = \sqrt{\frac{2J+1}{8\pi^2}}D^{J*}_{Kk}$, with D^J_{KM} as the Wigner function. $c^{J_{tot}MK\varepsilon}_{n_R n_r n_\rho n_\gamma Jk}(t)$ are time-dependent coefficients. n_R, n_r, n_ρ, and n_γ label the basis functions of R, r, ρ, and γ, respectively. $G_{n_R}(R)$ are sine basis functions. $F_{n_r}(r)$, $Q_{n_\rho}(\rho)$, and $H_{n_\gamma}(\gamma)$ are the eigenfunctions of one-dimensional reference Hamiltonians. J_{tot} is the total angular momentum number of the system. M and K are the projections of J_{tot} on the space fixed (SF) and the BF z-axis, respectively. J is the angular momentum quantum number of CH_3I, and k is its projection of J on the C_{3v} symmetry axis.

The initial wave packet is constructed as the direct product of a localized wave packet $G^0(R)$ and the eigenfunction of CH_3I. The initial state of CH_3I is specified by the quantum numbers (n_0, J_0, k_0, K_0, p_0), representing the initial vibrational state, the initial rotational state of CH_3I, the projection of J_0 onto the C_{3v} symmetry axis, the projection of J_{tot} onto the BF

https://doi.org/10.1021/acs.jpca.5c03163
J. Phys. Chem. A 2025, 129, 6344−6349

z-axis, and the parity of CH_3I, respectively. $G^0(R)$ is chosen as a Gaussian function:

$$G^0(R) = (\pi\delta^2)^{-1/4}\exp\left[-\frac{(R-R_0)^2}{2\delta^2}\right]\exp\left(-i\sqrt{2\mu_R E_0}R\right) \quad (8)$$

where R_0 and δ are the Gaussian center and width, and E_0 is the mean collision energy. The split operator method is employed in the time-dependent propagation.[41]

The QD integral cross section (ICS) for a specific reactant ro-vibrational state is obtained by summing the total reaction probabilities over all the partial waves

$$\sigma_{v_{j_1}v_{j_2}}(E_{col}) = \frac{1}{(2j_1+1)(2j_2+1)}\frac{\pi}{2\mu_R E_{col}}\sum_J (2J+1) P^J_{v_{j_1}v_{j_2}}(E_{col}) \quad (9)$$

where E_{col} denotes the collision energy. Here, partial waves with $J > 0$ are treated within the centrifugal-sudden (CS) approximation.[42,43] The maximum J value is determined to be 720 to give converged ICSs.

An L-shaped grid is implemented to reduce the basis-set size.[44] The motion along the coordinate R is represented by 1500 sine basis functions in the whole range from 3.0 to 45.0 bohr, with 500 nodes in the interaction region. The motion along the coordinate r uses 26 basis functions in the asymptotic region and 70 in the interaction region. The rotational basis size is governed by $j = 330$, yielding a number of 7.27×10^8.

3. QUASI-CLASSICAL TRAJECTORY METHOD

QCT calculations utilize the VENUS96 software.[45] The ICS at a specific collision energy is computed as

$$\sigma(E_{col}) = \pi b_{max}^2 \frac{N_r}{N_{tot}} \quad (10)$$

where N_{tot} and N_r are the number of total and reactive trajectories, respectively. b_{max} is the maximum impact parameter, which is determined by using small batches of trajectories with trial values. The impact parameter b in the calculations is sampled by $b = R^{1/2}b_{max}$, in which R is a uniform random number in [0,1]. The relative statistical error is defined as $\Delta = \sqrt{(N_{tot}-N_r)/N_{tot}N_r}$.

Based on convergence tests, trajectories initiate from an initial reactant separation of 25 Å and terminate when the product or reactant separation reaches 8.0 Å. A time step of 0.05 fs is used to conserve the energy better than 1×10^{-4} kcal mol^{-1}. 100,000 trajectories are launched, yielding a relative statistical error below 5%.

4. RESULTS AND DISCUSSION

4.1. Total Reaction Probabilities. The notation (n_1, n_2, n_3) denotes quantum numbers for the CH_3 symmetric stretching, CH_3 umbrella, and C−I stretching modes of the reactant CH_3I. Eight initial states are considered: (1) the ground vibrational state, (0,0,0), with a zero-point energy of 2443.97 cm^{-1} (0.303 eV), (2) the fundamental and first overtone of the umbrella mode, (0,1,0) and (0,2,0), having excitation energies of 1258.37 cm^{-1} (0.156 eV) and 2502.37 cm^{-1} (0.310 eV), (3) the fundamental of the C−I stretching mode, (0,0,1), with an excitation energy of 540.48 cm^{-1} (0.067 eV), (4) the fundamental of the CH_3 symmetric stretching mode, (1,0,0), with an excitation energy of 3054.06 cm^{-1} (0.379 eV), (5) the combination state involving CH_3 stretching and umbrella excitation, (1,1,0), having an excitation energy of at 4311.87 cm^{-1} (0.535 eV), and (6) the combination states, (0,1,1) and (1,0,1), with excitation energies of 1793.92 cm^{-1} (0.222 eV) and 3594.08 cm^{-1} (0.446 eV). The excitation energies are listed in Table 1.

Table 1. Excitation Energies of the Eight Initial States[a]

state	cm^{-1}	eV
(0,0,0)	2443.97	0.303
(0,0,1)	540.48	0.067
(0,1,0)	1258.37	0.156
(0,1,1)	1793.92	0.222
(0,2,0)	2502.37	0.310
(1,0,0)	3054.06	0.379
(1,0,1)	3594.08	0.446
(1,1,0)	4311.87	0.535

[a]The values of (0,0,0) represent the zero-point energies.

Figure 2 shows the total reaction probabilities with $J_{tot} = 0$ for the title reaction as a function of collision energy from the

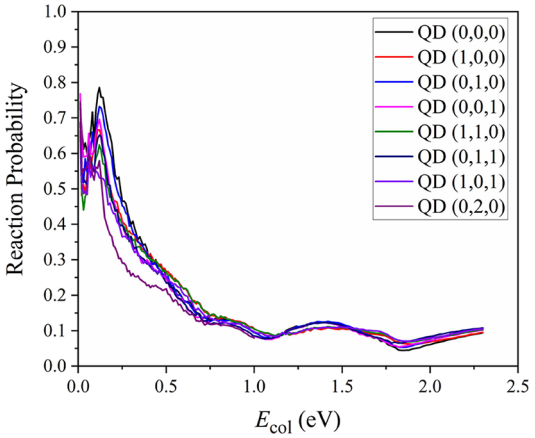

Figure 2. QD reaction probabilities from several selected initial states, labeled as (v_1, v_2, v_3), for the $F^- + CH_3I \rightarrow CH_3F + I^-$ S_N2 reaction with the total angular momentum $J_{tot} = 0$ as a function of collision energy.

eight selected initial states of the reactant CH_3I. All the probability curves give a similar collision energy dependence; i.e., they first decrease sharply with the increase of the collision energy, second rise up, then descend again, and finally become more or less flat as the collision energy further increases. Vibrational excitation of the C−I stretching mode, CH_3 symmetric stretching, or CH_3 umbrella mode slightly inhibits the reaction at low collision energies while modestly enhancing the reaction at relatively high collision energies. In contrast, the probability curves are crossed at mediate collision energies. Moreover, the calculated reaction probabilities from the eight initial states all oscillate visibly at low collision energies below about 0.75 eV, implying the existence of a significant quantum effect.

4.2. Reaction Mechanism. To gain mechanistic insight into the title reaction, the corresponding QCT reaction probabilities from the ground state are computed with zero impact parameters, as shown in Figure 3. The total QCT

https://doi.org/10.1021/acs.jpca.5c03163
J. Phys. Chem. A 2025, 129, 6344−6349

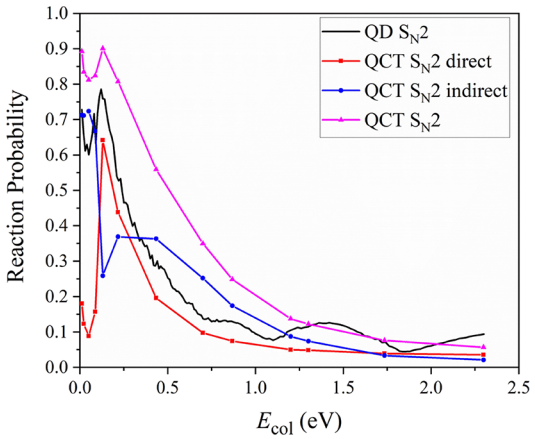

Figure 3. Mechanism-specific ground-state QCT reaction probabilities (J_{tot} = 0) as a function of collision energy for the F^- + CH_3I S_N2 reaction.

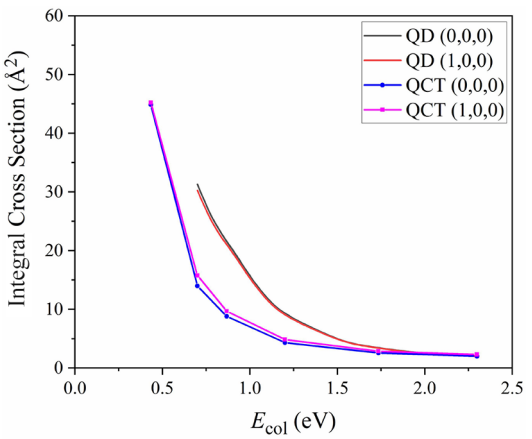

Figure 4. QD and QCT integral cross sections as a function of the collision energy for the F^- + CH_3I S_N2 reaction.

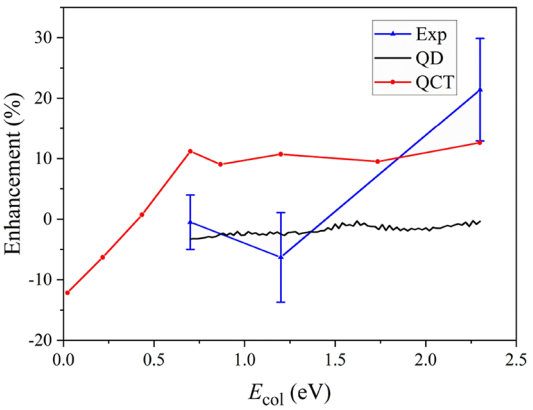

Figure 5. QD and QCT reaction probability ratios between vibrationally excited and ground-state CH_3I as a function of collision energy for the F^- + CH_3I S_N2 reaction.

probabilities show the same trend as the QD results. The reaction can proceed by either direct or indirect mechanisms, which are identified by the reaction time or the product translational energy. The proportion of direct versus indirect trajectories, categorized by reaction time, for the ground-state reaction is displayed in the same figure. The reaction is dominated by the indirect mechanism at very low energies, possibly caused by the trapping in the prereaction well. The indirect reaction probability first drops to a local minimum near E_{col} = 0.13 eV, then increases with the collision energy, reaches a local maximum at about E_{col} = 0.21 eV, and finally decreases with increasing E_{col}. In contrast, the direct reaction probability first decreases, then increases with the collision energy, reaches a maximum around E_{col} = 0.13 eV, and finally decreases with increasing E_{col}. The reaction almost follows the minimum energy path at low collision energies. The increased collision energy enhances the direct reactions by avoiding the formation of a prereactive complex and thus inhibits the indirect reactions. At even higher energies, however, the fast-moving F^- makes trapping of CH_3I difficult. In addition, the first kink in the QD probability curve at extremely low collision energies is obviously caused by the direct reaction mechanism, which differs from what was observed in the F^- + CH_3Cl reaction, in which the kink was attributed to the competition of the direct and indirect mechanisms.[21] Considering that the Walden-inversion reaction pathway of the F^- + CH_3I reaction is similar to that of F^- + CH_3Cl, the discrepancy possibly results from the mass difference between CH_3I and CH_3Cl.

4.3. Integral Cross Sections. Roland Wester's group have investigated the influence of symmetric C−H stretching vibration on the reaction of F^- with CH_3I over a collision energy range of 0.7−2.3 eV using an ion−molecule crossed-beam imaging spectrometer.[23] They found that for the nucleophilic substitution channel, the spectator-like CH stretching mode at low collision energies transitions to promoting the reaction at higher collision energies. The ICSs from the reactant ground state (0,0,0) and the fundamental state of the CH_3 symmetric stretching mode are calculated by both QD and QCT methods, as shown in Figure 4, and compared with experimental results on the enhancement in Figure 5. The analysis of the QD opacity functions reveals that the reaction is dominated by large partial-wave collisions. As a result, the low-J reaction probabilities contribute minimally to the integral cross section. As can be seen from Figure 4, the ICSs from the (0,0,0) and (1,0,0) states resemble each other very much for both QD and QCT calculations, which decrease monotonically with increasing collision energy, being a characteristic of barrierless reactions. It can also be noted that the QCT ICSs are visibly smaller than the corresponding QD ones at low collision energies, and the difference between them decreases as the collision energy increases. The difference possibly results from the approximations in both the QCT and QD methods. It is well-known that the QCT method has inherent drawbacks, such as the neglect of the quantum effect and the leakage of zero-point energy. The quantum effect is expected to be significant at low collision energies. On the other hand, the reduced-dimensional model employed in the QD calculations could bring about some uncertainty in the result as well.

Experimentally, a change of −0.5 ± 4.5, −6.3 ± 7.4, and +21.4 ± 8.5% in reactivity for the S_N2 channel due to the excited CH stretching vibration was observed at 0.7, 1.2, and 2.3 eV, respectively, which indicated that the S_N2 channel is not visibly affected by vibrationally exciting the CH_3 symmetric stretching mode at low collision energies, while it becomes significantly enhanced at high collision energies.[23] As can be seen from Figure 5, the QD calculations show a subtle inhibition effect at low collision energies, consistent with the experimental result. However, the promotional effect at high collision energies is not reproduced by the QD calculations,

https://doi.org/10.1021/acs.jpca.5c03163
J. Phys. Chem. A 2025, 129, 6344−6349

which, however, predicts a tiny inhibition effect. In contrast, the QCT calculations imply an enhancement effect at high collision energies, in agreement with the experimental result. The discrepancy between theoretical and experimental results is tentatively attributed to the inherent drawbacks of the QCT method and the reduced-dimensional model employed in the QD calculations.

5. CONCLUSIONS

In this work, we present a reduced six-dimensional quantum dynamical and full-dimensional quasi-classical trajectory study of the dynamics of the $F^- + CH_3I \rightarrow I^- + CH_3F$ S_N2 reaction on an accurate global PES. Specifically, the six-dimensional model enables studying the influence of three vibrational modes, namely, the C−I vibration, the CH_3 umbrella mode, and the CH_3 stretching vibrations, on the reactivity. The reaction probabilities from the several selected initial vibrational states of CH_3I all have an interesting collision energy dependence, apparently due to the competition of the direct and indirect reaction mechanisms. Vibrational excitation of reactant CH_3I has little effect on the reactivity.

AUTHOR INFORMATION

Corresponding Authors

Yan Wang − *School of Chemical and Environmental Engineering, Hubei Minzu University, Enshi 445000, China;* orcid.org/0009-0008-8199-5156; Email: hbwangy@sohu.com

Gábor Czakó − *MTA-SZTE Lendület "Momentum" Computational Reaction Dynamics Research Group, Interdisciplinary Excellence Centre and Department of Physical Chemistry and Materials Science, Institute of Chemistry, University of Szeged, H-6720 Szeged, Hungary;* orcid.org/0000-0001-5136-4777; Email: gczako@chem.u-szeged.hu

Authors

Zhao Tu − *School of Chemical and Environmental Engineering, Hubei Minzu University, Enshi 445000, China; Key Laboratory of Magnetic Resonance in Biological Systems, National Center for Magnetic Resonance in Wuhan, State Key Laboratory of Magnetic Resonance and Atomic and Molecular Physics, Innovation Academy for Precision Measurement Science and Technology, Chinese Academy of Sciences, Wuhan 430071, China;* orcid.org/0009-0006-7740-1592

Hongwei Song − *Key Laboratory of Magnetic Resonance in Biological Systems, National Center for Magnetic Resonance in Wuhan, State Key Laboratory of Magnetic Resonance and Atomic and Molecular Physics, Innovation Academy for Precision Measurement Science and Technology, Chinese Academy of Sciences, Wuhan 430071, China;* orcid.org/0000-0001-8401-2364

Minghui Yang − *Key Laboratory of Magnetic Resonance in Biological Systems, National Center for Magnetic Resonance in Wuhan, State Key Laboratory of Magnetic Resonance and Atomic and Molecular Physics, Innovation Academy for Precision Measurement Science and Technology, Chinese Academy of Sciences, Wuhan 430071, China;* orcid.org/0000-0003-1067-2217

Complete contact information is available at: https://pubs.acs.org/10.1021/acs.jpca.5c03163

Notes

The authors declare no competing financial interest.

ACKNOWLEDGMENTS

This work was supported by the National Science Foundation of China (Grant No. 21963008 to Y.W). G.C. thanks the National Research, Development and Innovation Office—NKFIH, K-146759; project no. TKP2021-NVA-19, provided by the Ministry of Culture and Innovation of Hungary from the National Research, Development and Innovation Fund, financed under the TKP2021-NVA funding scheme; and the Momentum (Lendület) Program of the Hungarian Academy of Sciences for financial support.

REFERENCES

(1) Zare, R. N. Laser Control of Chemical Reactions. *Science* **1998**, *279*, 1875−1879.

(2) Crim, F. F. Chemical Dynamics of Vibrationally Excited Molecules: Controlling Reactions in Gases and on Surfaces. *Proc. Natl. Acad. Sci. U. S. A.* **2008**, *105* (35), 12654−12661.

(3) Czakó, G.; Bowman, J. M. Reaction Dynamics of Methane with F, O, Cl, and Br on ab Initio Potential Energy Surfaces. *J. Phys. Chem. A* **2014**, *118* (16), 2839−2864.

(4) Guo, H.; Liu, K. Control of Chemical Reactivity by Transition-state and Beyond. *Chem. Sci.* **2016**, *7* (7), 3992−4003.

(5) Liu, K. Vibrational Control of Bimolecular Reactions with Methane by Mode, Bond, and Stereo Selectivity. *Annu. Rev. Phys. Chem.* **2016**, *67* (1), 91−111.

(6) Zheng, R.; Zhu, Y.; Song, H. Mode-specific Quantum Dynamics and Kinetics of the Hydrogen Abstraction Reaction $OH + H_2O \rightarrow H_2O + OH$. *Phys. Chem. Chem. Phys.* **2019**, *21* (43), 24054−24060.

(7) Zhang, D. H.; Guo, H. Recent Advances in Quantum Dynamics of Bimolecular Reactions. *Annu. Rev. Phys. Chem.* **2016**, *67* (1), 135−158.

(8) Fu, B.; Shan, X.; Zhang, D. H.; Clary, D. C. Recent Advances in Quantum Scattering Calculations on Polyatomic Bimolecular Reactions. *Chem. Soc. Rev.* **2017**, *46* (24), 7625−7649.

(9) Liu, Y.; Song, H.; Xie, D.; Li, J.; Guo, H. Mode Specificity in the $OH + HO_2 \rightarrow H_2O + O_2$ Reaction: Enhancement of Reactivity by Exciting a Spectator Mode. *J. Am. Chem. Soc.* **2020**, *142* (7), 3331−3335.

(10) Papp, P.; Czakó, G. Rotational Mode Specificity in the $F^- + CH_3I(v = 0, JK)$ S_N2 and Proton-Transfer Reactions. *J. Phys. Chem. A* **2020**, *124* (43), 8943−8948.

(11) Song, H.; Xie, W.; Zhang, C.; Yang, M. Toward a Comprehensive Understanding of Mode-Specific Dynamics of Polyatomic Reactions: A Full-Dimensional Quantum Dynamics Study of the $H + NH_3$ Reaction. *J. Phys. Chem. A* **2022**, *126* (5), 663−669.

(12) Polanyi, J. C. Concepts in Reaction Dynamics. *Acc. Chem. Res.* **1972**, *5* (5), 161−168.

(13) Welsch, R.; Manthe, U. Full-dimensional and Reduced-dimensional Calculations of Initial State-selected Reaction Probabilities Studying the $H + CH_4 \rightarrow H_2 + CH_3$ Reaction on a Neural Network PES. *J. Chem. Phys.* **2015**, *142* (6), No. 064309.

(14) Ellerbrock, R.; Manthe, U. Communication: Reactivity Borrowing in the Mode Selective Chemistry of $H + CHD_3 \rightarrow H_2 + CD_3$. *J. Chem. Phys.* **2017**, *147* (24), 241104.

(15) Liu, R.; Song, H.; Qi, J.; Yang, M. A Ten-dimensional Quantum Dynamics Model for the $X + YCAB_2$ Reaction: Application to $H + CH_4$ Reaction. *J. Chem. Phys.* **2020**, *153* (22), 224119.

(16) Li, J.; Jiang, B.; Song, H.; Ma, J.; Zhao, B.; Dawes, R.; Guo, H. From ab Initio Potential Energy Surfaces to State-Resolved Reactivities: $X + H_2O \leftrightarrow HX + OH$ [X = F, Cl, and $O(^3P)$] Reactions. *J. Phys. Chem. A* **2015**, *119* (20), 4667−4687.

(17) Pan, H.; Liu, K. State-to-State Dynamics in Mode-Specific Reactions of Cl + $CH_3D(v_1$-I, v_1-II, and v_4=1; |10⟩): Loss of Memory or Not. *J. Phys. Chem. Lett.* **2023**, *14* (7), 1769−1776.
(18) Czakó, G.; Gruber, B.; Papp, D.; Tajti, V.; Tasi, D. A.; Yin, C. First-principles Mode-specific Reaction Dynamics. *Phys. Chem. Chem. Phys.* **2024**, *26* (22), 15818−15830.
(19) Song, H.; Guo, H. Theoretical Insights into the Dynamics of Gas-phase Bimolecular Reactions with Submerged Barriers. *ACS Phys. Chem. Au.* **2023**, *3* (5), 406−418.
(20) Tasi, D. A.; Czakó, G. Vibrational Mode-specificity in the Dynamics of the OH^- + CH_3I Multi-channel Reaction. *J. Chem. Phys.* **2024**, *160* (4), No. 044305.
(21) Wang, Y.; Song, H.; Szabó, I.; Czakó, G.; Guo, H.; Yang, M. Mode-Specific S_N2 Reaction Dynamics. *J. Phys. Chem. Lett.* **2016**, *7* (17), 3322−3327.
(22) Olasz, B.; Szabó, I.; Czakó, G. High-level ab Initio Potential Energy Surface and Dynamics of the F^- + CH_3I S_N2 and Proton-transfer Reactions. *Chem. Sci.* **2017**, *8* (4), 3164−3170.
(23) Michaelsen, T.; Bastian, B.; Ayasli, A.; Strübin, P.; Meyer, J.; Wester, R. Influence of Vibrational Excitation on the Reaction of F^- with CH_3I: Spectator Mode Behavior, Enhancement, and Suppression. *J. Phys. Chem. Lett.* **2020**, *11* (11), 4331−4336.
(24) Stei, M.; Carrascosa, E.; Dörfler, A.; Meyer, J.; Olasz, B.; Czakó, G.; Li, A.; Guo, H.; Wester, R. Stretching Vibration is a Spectator in Nucleophilic Substitution. *Sci. Adv.* **2018**, *4* (7), No. eaas9544.
(25) Li, Y.; Wang, Y.; Wang, D. Quantum Dynamics Study of the Potential Energy Minima Effect on Energy Efficiency for the F^- + CH_3Cl → FCH_3 + Cl^- Reaction. *J. Phys. Chem. A* **2017**, *121* (14), 2773−2779.
(26) Ma, X.; Tan, X.; Hase, W. L. Effects of Vibrational and Rotational Energies on the Lifetime of the Pre-reaction Complex for the F^-+ CH_3I S_N2 Reaction. *Int. J. Mass Spectrom.* **2018**, *429*, 127−135.
(27) Schmatz, S. Quantum Dynamics of Gas-Phase S_N2 Reactions. *ChemPhysChem* **2004**, *5* (5), 600−617.
(28) Olasz, B.; Czakó, G. Mode-Specific Quasiclassical Dynamics of the F^-+ CH_3I S_N2 and Proton-Transfer Reactions. *J. Phys. Chem. A* **2018**, *122* (41), 8143−8151.
(29) Szabó, I.; Császár, A. G.; Czakó, G. Dynamics of the F^- + CH_3Cl → Cl^- + CH_3F S_N2 Reaction on a Chemically Accurate Potential Energy Surface. *Chem. Sci.* **2013**, *4* (12), 4362.
(30) Szabó, I.; Czakó, G. Revealing a Double-inversion Mechanism for the F^- + CH_3Cl S_N2 Reaction. *Nat. Commun.* **2015**, *6* (1), 5972.
(31) Szabó, I.; Czakó, G. Benchmark ab Initio Characterization of the Complex Potential Energy Surface of the Cl^- + CH_3I Reaction. *J. Phys. Chem. A* **2017**, *121* (30), 5748−5757.
(32) Nacsa, A. B.; Tajti, V.; Czakó, G. Dynamics of the Cl^- + CH_3I Reaction on a High-level ab Initio Analytical Potential Energy Surface. *J. Chem. Phys.* **2023**, *158* (19), 194306.
(33) Szabó, I.; Telekes, H.; Czakó, G. Accurate ab Initio Potential Energy Surface, Thermochemistry, and Dynamics of the F^-+ CH_3F S_N2 and Proton-abstraction Reactions. *J. Chem. Phys.* **2015**, *142* (24), 244301.
(34) Vande Linde, S. R.; Hase, W. L. A Direct Mechanism for S_N2 Nucleophilic Substitution Enhanced by Mode-selective Vibrational Excitation. *J. Am. Chem. Soc.* **1989**, *111* (6), 2349−2351.
(35) Hase, W. L. Simulations of Gas-Phase Chemical Reactions: Applications to S_N2 Nucleophilic Substitution. *Science* **1994**, *266* (5187), 998−1002.
(36) Viggiano, A. A.; Morris, R. A.; Paschkewitz, J. S.; Paulson, J. F. Kinetics of the Gas-phase Reactions of Chloride Anion, Cl^- with CH_3Br and CD_3Br: Experimental Evidence for Nonstatistical Behavior? *J. Am. Chem. Soc.* **1992**, *114* (26), 10477−10482.
(37) Ayotte, P.; Kim, J.; Kelley, J. A.; Nielsen, S. B.; Johnson, M. A. Photoactivation of the Cl^- + CH_3 Br S_N2 Reaction via Rotationally Resolved C−H Stretch Excitation of the Cl^-·CH_3Br Entrance Channel Complex. *J. Am. Chem. Soc.* **1999**, *121* (29), 6950−6951.
(38) Tonner, D. S.; McMahon, T. B. Non-Statistical Effects in the Gas Phase S_N2 Reaction. *J. Am. Chem. Soc.* **2000**, *122* (36), 8783−8784.
(39) Kowalewski, M.; Mikosch, J.; Wester, R.; De Vivie-Riedle, R. Nucleophilic Substitution Dynamics: Comparing Wave Packet Calculations with Experiment. *J. Phys. Chem. A* **2014**, *118* (26), 4661−4669.
(40) Ayasli, A.; Khan, A.; Gstir, T.; Michaelsen, T.; Papp, D.; Wang, Y.; Song, H.; Yang, M.; Czakó, G.; Wester, R. A Dynamic Isotope Effect in the Nucleophilic Substitution Reaction Between F^- and CD_3I. *Nat. Commun.* **2025**, *16* (1), 2318.
(41) Fleck, J. A.; Morris, J.; Feit, M. Time-dependent Propagation of High Energy Laser Beams Through the Atmosphere. *Appl. Phys.* **1976**, *10*, 129−160.
(42) Pack, R. T. Space-fixed vs Body-fixed Axes in Atom-diatomic Molecule Scattering. *Sudden Approximations. J. Chem. Phys.* **1974**, *60* (2), 633−639.
(43) McGuire, P.; Kouri, D. J. Quantum Mechanical Close Coupling Approach to Molecular Collisions. jz-conserving Coupled States Approximation. *J. Chem. Phys.* **1974**, *60* (6), 2488−2499.
(44) Zhang, D. H.; Zhang, J. Z. H. Accurate Quantum Calculation for the Benchmark Reaction H_2 + OH → H_2O + H in Five-dimensional Space: Reaction Probabilities for J = 0. *J. Chem. Phys.* **1993**, *99* (7), 5615−5618.
(45) Hase, W. L.; Duchovic, R. J.; Hu, X.; Komornicki, A.; Lim, K.; Lu, D. H.; Peslherbe, G. H.; Swamy, K. N.; Vande Linde, S.; Varandas, A. VENUS96: A General Chemical Dynamics Computer Program. *Quantum Chem. Program Exch. Bull.* **1996**, *16* (4), 43.

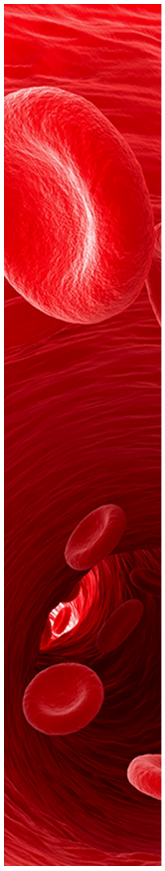
CAS BIOFINDER DISCOVERY PLATFORM™
CAS BIOFINDER HELPS YOU FIND YOUR NEXT BREAKTHROUGH FASTER
Navigate pathways, targets, and diseases with precision
Explore CAS BioFinder
CAS
A division of the American Chemical Society

https://doi.org/10.1021/acs.jpca.5c03163
J. Phys. Chem. A 2025, 129, 6344−6349